HYDROTHERMAL SYNTHESIS AND OPTICAL PROPERTIES OF $CuInS_2$ MICRO-/NANOMATERIALS BY USING GEMINI SURFACTANT AS SOFT TEMPLATE [**]

Wen-Gui Chang[*], Li-Li Tao

West Anhui University, Department of Materials and Chemical Engineering, Anhui Province Laboratory of Biomimetic Sensor and Detecting Techniques, Lu'an 237012, China; e-mail: wgchang1018@163.com

We demonstrate in this paper the shape-controlled synthesis of $CuInS_2$ micro-/nanoparticles through a facile hydrothermal method. Samples with different morphologies, i.e., nanoparticles and porous microspheres, are hydrothermally prepared in the presence of Gemini surfactant 1,10-bis(4-methyl-4-hexadecylpiperazine)decamethylene dibromide (Pi-16-10-16) as soft template. The products were characterized by using SEM, XRD, XPS, and EDS. Furthermore, the charge-discharge capability of the as-prepared $CuInS_2$ samples is investigated by using the samples as the cathode in a lithium battery. The charge-discharge curves for the cells of $CuInS_2$ exhibit higher initial discharge capacity showing a discharge capacity of 673 mAh/g, which is important for potential applications in photovoltaic (PV) and photoelectrochemical areas.

Keywords: *$CuInS_2$, Gemini surfactant, controlled synthesis, electrical-optical property.*

ГИДРОТЕРМАЛЬНЫЙ СИНТЕЗ И ОПТИЧЕСКИЕ СВОЙСТВА МИКРО-/НАНОМАТЕРИАЛОВ $CuInS_2$, ПОЛУЧЕННЫХ С ИСПОЛЬЗОВАНИЕМ ПОВЕРХНОСТНО-АКТИВНОГО ВЕЩЕСТВА ДЖЕМИНИ В КАЧЕСТВЕ МЯГКОЙ МАТРИЦЫ

W.-G. Chang[*], L.-L. Tao

УДК 620.3;543.422.8

Университет Западного Аньхоя, Луан, 237012, Китай; e-mail: wgchang1018@163.com

(Поступила 7 мая 2018)

Синтезированы микро-/наночастицы $CuInS_2$ контролируемой формы с помощью простого гидротермального метода. Образцы с различной морфологией, а именно наночастицы и пористые микросферы, готовили гидротермически в присутствии поверхностно-активного вещества Gemini (1,10-бис-(4-метил-4-гексадецилпиперазин)декаметилдибромида) (Pi-16-10-16) в качестве мягкой матрицы. Продукты синтеза исследованы с помощью сканирующей электронной микроскопии, рентгеновской дифракции, рентгеновской фотоэлектронной спектроскопии и энергодисперсионной рентгеновской спектроскопии. Исследована способность свежеприготовленных образцов $CuInS_2$ к разряду/заряду при использовании их в качестве катода в литиевой батарее. Кривые заряда/разряда для ячеек $CuInS_2$ показали высокую начальную емкость разряда 673 мАч/г, что важно для потенциальных применений в фотовольтаике и фотоэлектрохимии.

Ключевые слова: *$CuInS_2$, поверхностно-активное вещество Gemini, управляемый синтез, электрооптические свойства.*

Introduction. I-III-VI_2 chalcopyrite structure compounds have attracted extensive attention over the last two decades because of their tunable electronic and optical properties [1, 2]. As a typical ternary chalcopyrite material, $CuInS_2$ has been considered as one of the most popular and promising candidates as ab-

[**] Full text is published in JAS V. 86, No. 3 (http://springer.com/10812) and in electronic version of ZhPS V. 86, No. 3 (http://www.elibrary.ru/title_about.asp?id=7318; sales@elibrary.ru).

sorber materials for photovoltaic applications because of its high absorption coefficient and environmental consideration [3]. The band gap of $CuInS_2$ is 1.55 eV, which is very near the optimum band gap for solar cells. Solar cells fabricated with $CuInS_2$ thin films have already exhibited an efficiency of 16% on an area of 1 cm^2 [4]. The device properties of $CuInS_2$-based solar cells are highly affected by their stoichiometric composition [5–7]. In contrast to the physical and chemical vapor deposition techniques, the hydrothermal method is a simple and inexpensive technique in which the ratios of the constituents are controlled by adjusting their molar ratios in the solution. Of all the synthetic methods that have been evaluated [8], the most classical preparative studies have been conducted on $CuInS_2$ produced via spray pyrolysis, rf sputtering, sulfurization, electrodeposition, and chemical processes. Various $CuInS_2$ structures have been successfully fabricated [9–12]. Nevertheless, it is still a grand challenge to prepare $CuInS_2$ materials with controlled size and shape.

Gemini surfactants have two identical moieties connected at the level of the head groups by a spacer [13]. They possess several characteristics that make them superior to similar conventional surfactants and have many potential applications. An important characteristic of Gemini surfactants is that they can be used as a soft template in biomimetic synthesis to control the structure and morphology of the photoelectric inorganic nanomaterials. Although several studies have been conducted to evaluate the synthesis of porous materials MCM-48 [14] and photoelectric inorganic nanomaterials [15–17] using Gemini surfactant as a molecular template, the Gemini surfactants used as the soft template in those studies were all cationic tertiary amine Gemini surfactants, such as $C_{12\text{-}3\text{-}12}$ [15], and $C_{14\text{-}2\text{-}14}$ [17]. Conversely, there have been relatively few studies conducted to evaluate the synthesis of porous materials and nanoparticles using Gemini surfactant with a piperazine group as the template.

In this study, we synthesized Gemini surfactant Pi-16-10-16, then utilized it as the soft template in the controlled synthesis of $CuInS_2$ micro-/nanomaterials, and its electrical-optical properties were also investigated.

Experiment. 1,10-Dibromodecane (AR, A Johnson Matthey Company), 1-bromohexadecane, lauric acid, chlorosulfonic acid, *p*-aminobenzene sulfonic acid, phosphoric acid, hydrogen peroxide (H_2O_2, 30 wt.%), N-methylpiperazine, $Cu(NO_3)_2$, $InCl_3 \cdot 4H_2O$, thioacetamide (TAA), and anhydrous alcohol were purchased from the Chemical Reagent Co. Ltd. (Shanghai, China) and then used as received without further purification. All chemicals used in this study were of analytical grade and all water used was double distilled. Gemini surfactant Pi-16-10-16 was synthesized according to previously described methods [18, 19]. The surfactants were then utilized for subsequent procedures after repeated crystallization by anhydrous alcohol.

To synthesize $CuInS_2$, $Cu(NO_3)_2$, $InCl_3 \cdot 4H_2O$, TAA, and Gemini surfactant were mixed and added into a Teflon-lined steel autoclave, which was then filled with water up to 90% of the total volume. The autoclave was then sealed and maintained at 160^{o}C for 24 h and then air-cooled to room temperature. The black precipitates were then centrifuged and washed with double distilled water and anhydrous alcohol and then vacuum-dried at 60^{o}C for 4 h.

The as-prepared samples were characterized by X-ray powder diffraction (XRD) in a Rigaku D/max-γB X-ray diffractometer with a CuK_α radiation source (λ = 1.5418 Å) operated at 40 kV and 80 mA. Field-emission scanning electron microscopy (FESEM) was conducted using a Hitachi S-4800 scanning electron microscope. The Brunauer-Emmett-Teller (BET) surface area was determined by nitrogen adsorption (Micromeritics ASAP 2020 system). The X-ray photoelectron spectroscopy (XPS) spectra were recorded on a ESCALAB 250 (Thermo-VG Scientific) X-ray photoelectron spectrometer.

Results and discussion. Figure 1 shows the XRD patterns of the as-synthesized $CuInS_2$ obtained in the presence of Pi-16-10-16 at 160°C for different times. The diffraction peaks can be well indexed to tetragonal (space group: *P*) $CuInS_2$ with lattice parameters of a = 10.73 Å (JCPDS 75-0106). All products produced bulk patterns using Pi-16-10-16 as template, which indicates that all products are tetragonal phase $CuInS_2$ and that the templates have no significant effect on the crystal phase of $CuInS_2$.

Figures 2a–d show the FESEM images of as-synthesized $CuInS_2$ obtained in the presence of Gemini surfactant Pi-16-10-16 aged for different time. The as-synthesized $CuInS_2$ displayed morphologies of nanoparticles with the average size about 60 nm at the beginning of the reaction (Fig. 2a). With increasing aging time, the obtained $CuInS_2$ show morphologies of porous microspheres (Fig. 2b–d), the average diameter ranging for 1-4.0 μm when aged for 24 h (Fig. 2d). In comparison with Fig. 2a–d, the as-synthesized $CuInS_2$ show morphologies of porous microspheres by using Gemini surfactant Pi-16-10-16, which indicate that the Gemini surfactant played a key role in controlling the size and shape of $CuInS_2$ micro-/nanocrystals.

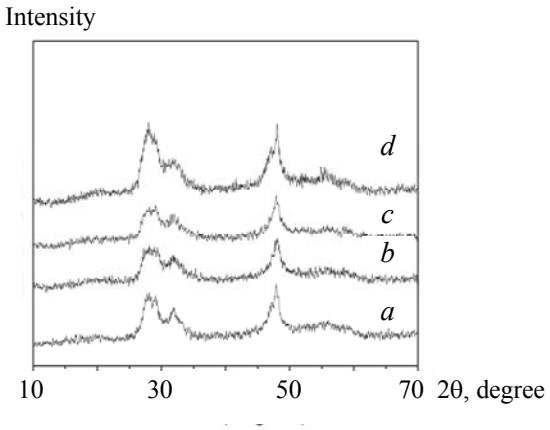

Fig. 1. XRD patterns of the as-synthesized $CuInS_2$ samples aged at 160°C for 4 (a), 8 (b), 12 (c), and 24 h (d).

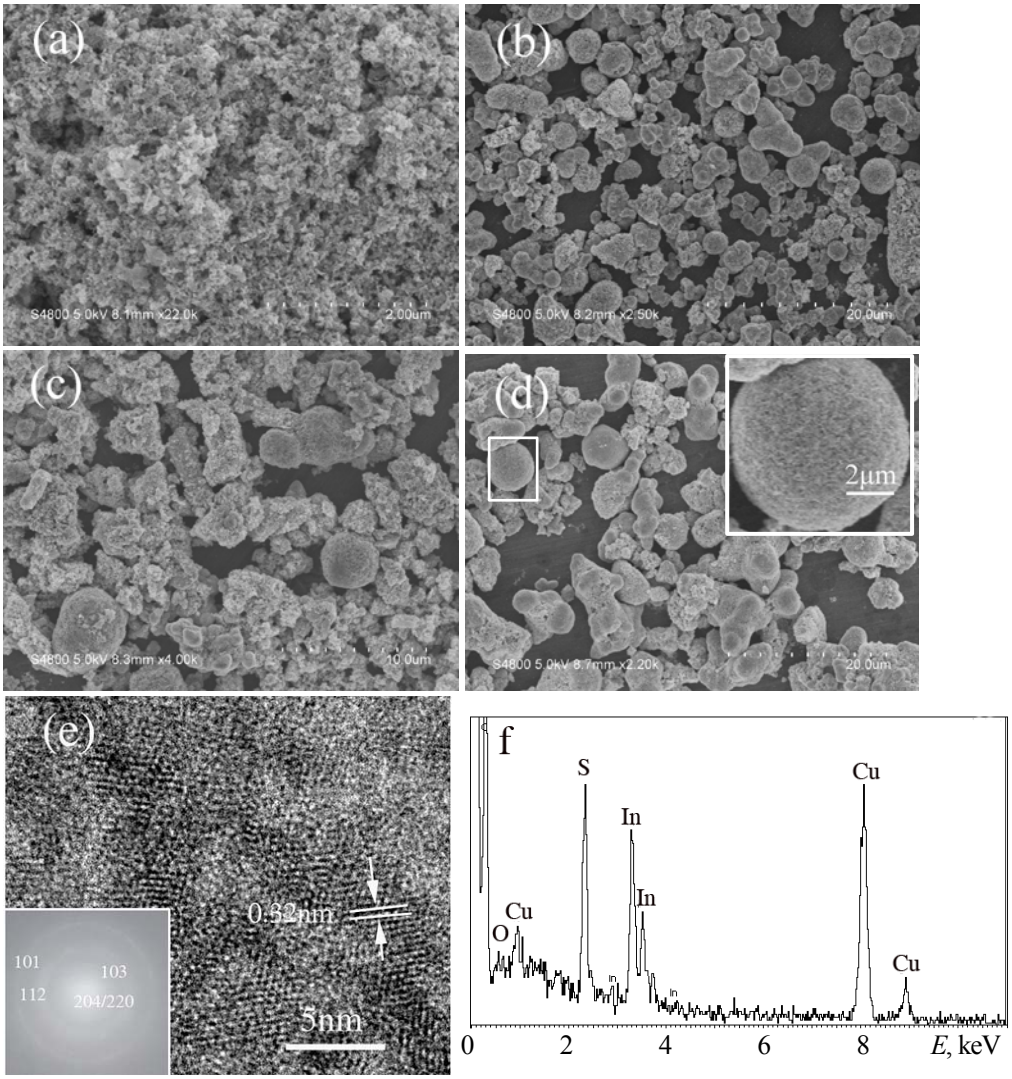

Fig. 2. FESEM images of the as-synthesized $CuInS_2$ samples incubated at 160°C for 4 (a), 8 (b), 12 (c), and 24 h (d), inset shows magnified image of the selected microsphere in the FESEM image of the as-obtained $CuInS_2$; (e) HRTEM image of the as-synthesized $CuInS_2$ products, inset shows the SAED pattern of the as-obtained $CuInS_2$ samples; (f) EDS spectrum of the as-obtained $CuInS_2$ samples.

Figure 2e and the inset show the typical HRTEM image and SAED pattern of the as-obtained $CuInS_2$ samples. The HRTEM image of the $CuInS_2$ microsphere shows the crystall structure and lattice fringes. The lattice fringes were measured as 0.32 nm, which corresponds to the (112) plane of the $CuInS_2$. The SAED pattern shows obvious polycrystalline rings that can be indexed to (101), (112), (103), and (204)/(220) facets of a tetragonal phase $CuInS_2$, which are in accord with the strongest diffraction peaks from XRD test (Fig. 1). Furthermore, the EDS analysis of the as-prepared $CuInS_2$ samples shown in Fig. 2f demonstrates that the chemical components only consisted of In, O, and S (the Cu signal arises from the TEM grid), suggesting the as-obtained product is CuInS, which is in agreement with the above XRD results.

Further evidence for the quality and composition of the samples is obtained by the XPS spectra of the products. Figure 3 show the XPS spectra of the $CuInS_2$ nano-/micro-particles obtained when Gemini surfactant Pi-16-10-16 was used as a template. The general scan spectra show the presence of strong C 1*s*, O 1*s*, Cu 2*p*, In 3*d*, and S 2*p* levels (Fig. 3a). There appears the characteristic peak of $CuLM_2$ at 918.10 eV, suggesting that the as-synthesized product was $CuLM_2$ type production structure. All peaks were calibrated using C 1*s* (284.6 eV) as the reference. Furthermore, the Cu 2*p* core level was split into $2p_{3/2}$ (931.90 eV) and $2p_{1/2}$ (951.60 eV) peaks (Fig. 3b), the In 3*d* core level was split into $3d_{5/2}$ (444.75 eV) and $3d_{3/2}$ (452.30 eV) peaks (Fig. 3c), while the S core showed a peak at 161.50 eV (Fig. 3d). All of the observed binding energy values for In 3*d* and S 2*p* were nearly in agreement with previously reported findings [20]. The contents of Cu, In, and S are quantified by Cu 2*p*, In 3*d*, and S 2*p* peak areas, and a molar ratio of 1.09:1:1.57 for Cu:In:S is given. Thus, the XPS results further prove that the sample is composed of $CuInS_2$.

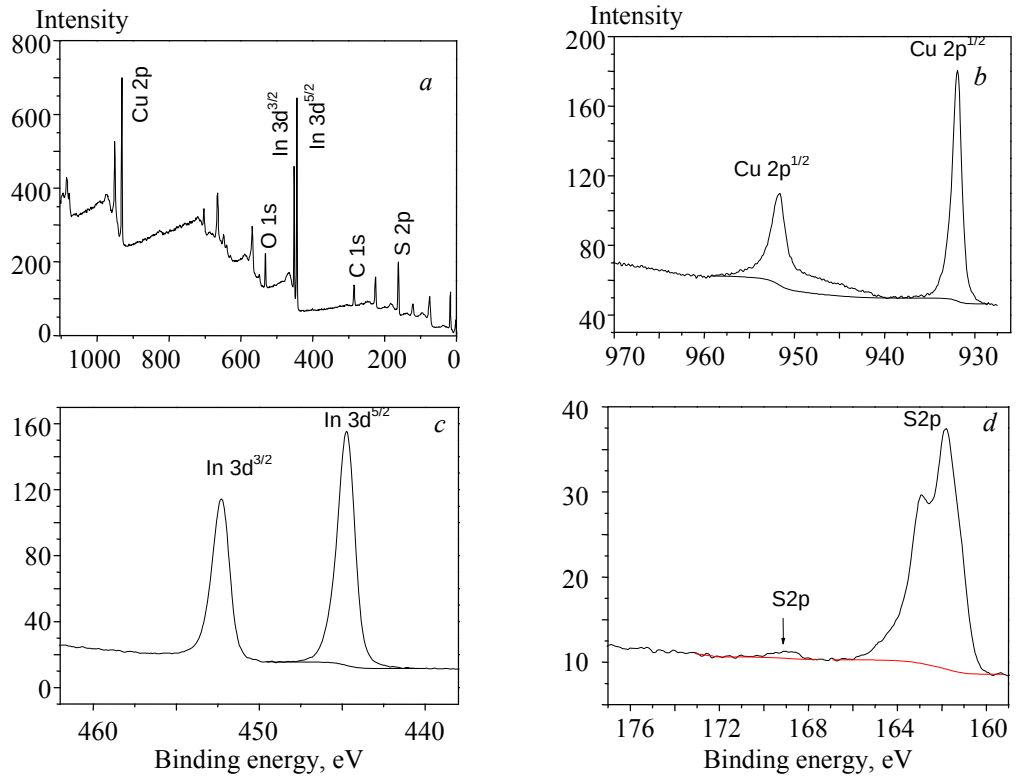

Fig. 3. XPS spectra of $CuInS_2$ micro-/nanoparticles obtained in the presence of Gemini surfactant as template incubated at 160°C for 1 h, (a) survey of the $CuInS_2$ NPs, (b) Cu 2*p*, (c) In 3*d*, (d) S 2*p*.

Figure 4a shows the nitrogen adsorption-desorption isotherms of $CuInS_2$ porous microspheres. The isotherms are of type IV, which confirms the characteristics of mesoporous materials. The Brunauer-Emmett-Teller (BET) of the sample is about 8.47 m^2/g. The Barrett-Joyner-Halenda (BJH) model analysis of these as-prepared porous microspheres is shown in the inset of Fig. 4a, which gives an average pore diameter of 364.28 nm and pore volume of 0.0953 cm^3/g. The larger pores result from the aggregation of nanoparticles of these porous microspheres, which indicates that they are not tightly bound to each other.

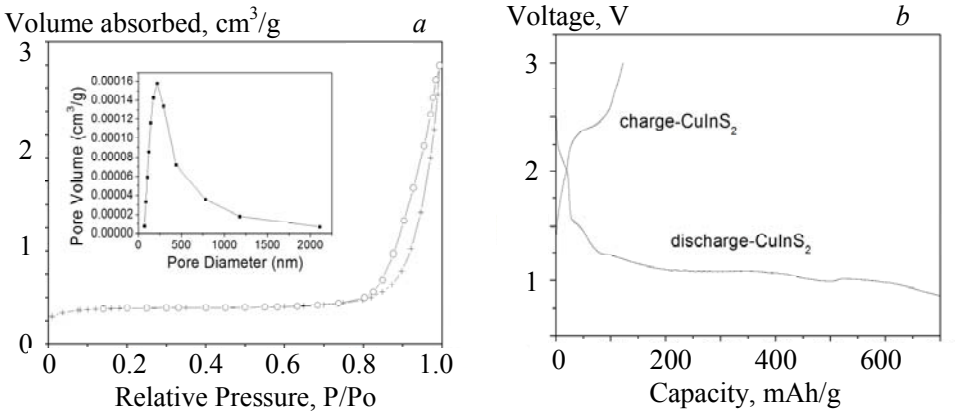

Fig. 4. N_2 adsorption-desorption isotherms of $CuInS_2$ products obtained in the presence of Gemini surfactant Pi-16-10-16 as template at 160°C for 24 h (a), inset shows pore diameter distributions (psd); charge-discharge curves in intial cycle of as-prepared $CuInS_2$ at a given constant current density of 0.5 mA/cm^2 (b).

The charge-discharge capability of the as-prepared $CuInS_2$ samples was investigated by using the samples as the cathode in a lithium battery. The curves of charge and discharge capacity for the cell (Fig. 4b) exhibit higher initial discharge capacity of 673 mAh/g. The initial electrochemical Li intercalation capacity is very close to the literature value [21], which indicates that this kind of $CuInS_2$ microstructure may be potentially applied as an electrode material in lithium ion battery.

Conclusion. We have successfully synthesized $CuInS_2$ micro-/nanoparticles through a facile hydrothermal method by using Gemini surfactant Pi-16-10-16 as soft template. The charge-discharge capability of the as-prepared $CuInS_2$ samples was investigated by using the samples as the cathode in a lithium ion battery. The charge-discharge for the cells exhibit higher initial discharge capacity of 673 mAh/g, which is important for potential photovoltaic (PV) and photoelectrochemical applications. Furthermore, the morphology and phase control of $CuInS_2$ nanostructures indicate that the Gemini surfactant plays a key role in controlling the size and shape of $CuInS_2$ micro-/nanocrystals. This method also opens a window for the application of the Gemini surfactants in the controlled synthesis of the nanomaterials.

Acknowledgment. This work was supported by the National Science Foundation of China (21271141), the National Science Foundation of Anhui Province (1308085ME57), Anhui Province Laboratory of Biomimetic Sensor and Detecting Techniques and Lu'an Engineering Technology Center of Fine Chemicals Engineering.

REFERENCES

1. X. L. Gou, F. Y. Cheng, Y. H. Shi, L. Zhang, S. J. Peng, J. Chen, P. W. Shen, *J. Am. Chem. Soc.*, **128**, 7222–7229 (2006).
2. D. C. Pan, L. J. An, Z. M. Sun, W. Hou, Y. Yang, Z. Z. Yang, Y. F. Lu, *J. Am. Chem. Soc.*, **130**, 5620–5621 (2008).
3. J. M. Peza-Tapia, A. Morales-Acevedo, M. Ortega-López, *Sol. Energ. Mater. Sol. Cells*, **93**, 544–548 (2009).
4. K. Das, S. K. Panda, S. Gorai, P. Mishra, S. Chaudhuri, *Mater. Res. Bull.*, **43**, 2742–2750 (2008).
5. J. E. Halpert, F. S. F. Morgenstern, B. Ehrler, Y. Vaynzof, D. Credgington, N. C. Greenham, *ACS Nano*, **9**, 5857–5867 (2015)
6. Y. Li, Y. Wang, R. Tang, X. Wang, P. Zhu, X. Zhao, C. Gao. *J. Phys. Chem. C*, **119**, 2963–2968 (2015).
7. W. Yue, F. Wei, C. He, D. Wu, N. Tang, Q. Qiao, *RSC Adv.*, **7**, 37578–37587 (2017).
8. S. J. Peng, J. Liang, L. Zhang, Y. H. Shi, J. Chen, *J. Cryst. Growth*, **305**, 99–103 (2007).
9. W. Yang, Y. Oh, J. Kim, H. Kim, H. Shin, J. Moon, *ACS Appl. Mater. Interfaces*, **8**, 425–431 (2016).
10. B. Chen, S. Chang, D. Li, L. Chen, Y. Wang, T. Chen, B. Zou, H. Zhong, A. L. Rogach, *Chem. Mater.*, **27**, 5949–5956 (2015).

11. W. C. Huang, C. H. Tseng, S. H. Chang, H. Y. Tuan, C. C. Chiang, L. M. Lyu, M. H. Huang, *Langmuir*, **28**, 8496–8501 (2012).
12. J. Zhang, W. Sun, L. Yin, X. Miao, D. Zhang, *J. Mater. Chem. C*, **2**, 4812–4817 (2014).
13. M. J. Rosen, D. J. Tracy, *J. Surfactant. Deterg*., **4**, 547–554 (1998).
14. K. Czechura, A. Sayari, *Chem. Mater*., **18**, 4147–4150 (2006).
15. M. S. Bakshi, P. Sharma, T. S. Banipal, *Mater. Lett.*, **61**, 5004–5009 (2007).
16. M. S. Bakshi, F. Possmayer, N. O. Petersen, *Chem. Mater*., **19**, 1257–1266 (2007).
17. M. S. Bakshi, F. Possmayer, N. O. Petersen, *J. Phys. Chem. C*, **112**, 8259–8265 (2008).
18. L. W. Zhao, H. L. Xie, J. Disper, *Sci. Technol*., **29**, 284–288 (2008).
19. Q. S. Zhang, H. M. Zhang, B. N. Guo, *Fine Chem*., **23**, 435–438 (2006).
20. Y. Liu, M. Zhang, Y. Q. Gao, R. Zhang, Y. T. Qian, *Mater. Chem. Phys*., **101**, 362–366 (2007).
21. Y. Liu, H. Y. Xu, Y. T. Qian, *Cryst. Growth Des*., **6**, 1304–1037 (2006).